The paper was published in the proceedings of the 11th International Conference on Physical Modelling in Geotechnics (ICPMG2026) and was edited by Ioannis Anastasopoulos. The conference was held from June 8th to June 12th 2026 in Zurich, Switzerland.

Proceedings of the 11th ICPMG 2026
11th International Conference on Physical Modelling in Geotechnics
8-12 June 2026, Zurich, Switzerland

Soil liquefaction triggered by ship waves in rivers and canals A laboratory investigation on fine sands

J. Rothschink (corresponding author), F.Karl, O.Stelzer
Federal Waterways Engineering and Research Institute, Karlsruhe, Germany, julia.rothschink@baw.de, fabian.karl@baw.de, oliver.stelzer@baw.de

ABSTRACT: In rivers and canals, typical linear water level drawdowns caused by ship waves can lead to liquefaction in the soil of riverbanks and bottoms. In this study, a sand sample in a cylindric test cell is subjected to real scale linear pressure changes where various external impact factors and boundary conditions that can cause or promote momentary liquefaction are considered. Excess pore water pressures are measured and critical gradients and effective stresses during a pressure change are calculated. The results show that liquefaction occurs, depending on the impact factors and boundary conditions. Yet there are still uncertainties considering the evaluation of liquefaction caused by a change in unit weight of the soil during liquefaction.

1 INTRODUCTION

In inland waterways, the banks and beds of rivers and canals are regularly subjected to ship waves. These cause pressure changes that affect the stress state in the soil and can lead to liquefaction, if the soil is not protected by a sufficient surface load. This can be the case if technical-biological bank protection using plants instead of riprap is used to protect the banks. Critical conditions can arise at the beginning of an installation of such measures, when the plants are still growing and cannot yet provide sufficient stability to the soil. Similarly, the riprap bank protection may be removed for the renaturation of a river. As these two cases will become more important in the future, it is crucial to understand the resulting processes in the soil during wave action.

Liquefaction generally occurs in saturated non-cohesive soils. Two mechanisms of lique-faction must be distinguished. On one hand shear-induced liquefaction (residual lique-faction) caused by e.g. earthquakes or vibrating loads which lead to pore water pressure accumulation in the soil (Terzaghi *et al.* 1967). And on the other hand momentary liquefaction (oscillatory liquefaction) which we will examine in more detail in this paper caused by a wave trough (Sakai *et al.* 1992). However, most of the research on momentary liquefaction focuses on ocean waves and the effects on the seabed (Nago 1981, Zen and Yamazaki 1990). To analyse the phenomena of ship-wave induced liquefaction in rivers under controlled boundary conditions in lab tests, the relevant parts of the ship-wave can be described as a linear water level drawdown (drawdown at bow and stern), characterized by a drawdown depth z_a and a drawdown time t_a, resulting in a drawdown velocity v_a as described in Federal Waterways Engineering and Research Institute (2010) (Figure 1). It is necessary to investigate which external factors and soil parameters enhance or reduce the potential of linear wave-induced liquefaction. In this paper, the focus is mainly on the external influencing factors, whereas the internal (soil) parameters are examined in Keese *et al.* (2026).

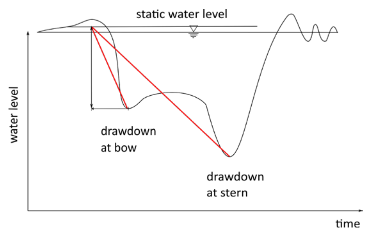

Figure 1: Simplified linear hydraulic pressure changes during typical ship waves in rivers and canals.

2 CRITERIA FOR WAVE INDUCED LIQUEFACTION

To understand liquefaction in soils caused by ship waves, we consider a quasi-saturated granular soil. It consists of a soil matrix and a compressible fluid phase (Skempton 1954, Fredlund 1976). The gas content in the pore water is assumed to be around 5-15 % (Köhler 1997). During a water level drawdown, the pressure in the quasi-saturated soil changes. This influences the gas phase, as the gas bubbles initially expand, as stated in Boyle's law, due to the decreasing pressure in the soil. As the gas bubbles expand, pore water in the pore space is displaced and flows towards the lower potential to compensate for the pressure change. If the permeability of the soil is significantly lower than the drawdown velocity, the displaced pore water cannot drain off quickly enough and excess pore water pressures can build up in the soil. When the excess pore water pressure reaches a critical value, the soil loses grain to grain contact and liquefaction occurs.

One definition of soil liquefaction in general is described with the failure criterion of the vertical effective stresses σ_v' (kPa) at a certain depth z (m) equal zero (Zen and Yamazaki 1990)

$$\sigma_v' = \sigma_v - p = z \cdot \gamma_{sat} - (\gamma_w \cdot z + \Delta p) = \gamma' \cdot z - \Delta p = 0 \quad (1)$$

With γ_{sat} (kN/m²) the saturated unit weight, σ_v (kPa) the total vertical stress, p (kPa) the total pore water pressure and Δp (kPa) the excess pore water pressure. γ' is the unit weight of the soil under buoyancy (kN/m²)

$$\gamma' = (\gamma_s - \gamma_w) \cdot (1 - n) \quad (2)$$

where γ_s is the grain unit weight (kN/m²), γ_w the unit weight of water (kN/m²) and n the porosity of the soil.

A second liquefaction criterion to validate the results is described by Terzaghi (Terzaghi *et al.* 1967) using the critical hydraulic gradient i_{crit}, which represents a limit hydraulic gradient depending on the porosity n of the soil. In this state, effective stresses are considered zero and grain-to-grain contacts are no longer present:

$$i_{crit} = \frac{\gamma'}{\gamma_w} = (1 - n) \cdot (\frac{\gamma_s}{\gamma_w} - 1) \quad (3)$$

If liquefaction occurs, the critical hydraulic gradient is reached over a certain time and not exceeded. If the liquefaction continues over a longer period of time, this is reflected in a plateau value of the critical hydraulic gradient (Terzaghi *et al.* 1967).

3 METHODS

For this study, liquefaction tests on a fine sand soil sample based on different boundary conditions were carried out, to observe and examine the potential of liquefaction. To provoke liquefaction, the sand samples were exposed to rapid linear water level drawdowns in a test apparatus (Figure 2 bottom, with initial state at t_0 (s) and end of the drawdown t_n (s)). The water level drawdowns were applied as pressure changes. By measuring the pressure within the soil sample, liquefaction can be detected by calculating the hydraulic gradient and the vertical effective stresses according to the criteria (eq. 1 and 3) described above.

3.1 Experimental Setup

To carry out the tests, the Alternating Flow Apparatus (Kayser *et al.* 2016) developed by the Federal Waterways Engineering and Research Institute is used. This apparatus consists of a test cell (Figure 2), 9 pressure sensors (pR10 (top) – pR90 (bottom)) along the cell, inductive flowmeters, two pressure tanks, equipped with dynamic pressure regulators and several flow pipes, leading from the tanks to the cell. The cell is filled with fine sand, which is pluviated into water, to create a quasi-saturated sample with a height of 0.86 m.

The cell allows water flow through the sample in both directions e.g. to determine permeability, but for the actual sunk tests, the lower boundary of the cell is closed. The upper boundary condition is open for inflow and outflow towards the corresponding pressure tank and the flow can be measured by the flowmeters. Pressure changes are initiated from above the sample.

Pressure values from 2 m to 90 m water level can be applied. The uppermost pressure sensor measures the pressure in the water, whereas the sensors beneath measure the pressure in the soil sample. Further information on the Alternating-Flow-Apparatus, the experimental setup and sample preparation can be found in Kayser *et al.* (2016) and Rothschink and Stelzer (2022). For this test series, no additional load on top of the sand sample is used, whereas in Rothschink and Stelzer (2022) a load is used to assure the stability, detect maximum excess pore water pressure and avoid liquefaction.

3.2 Study layout

The used material is Karlsruhe Fine sand, which is a quartz sand with a uniform sieve curve. For the built-in sand sample, the soil parameters (see Table 1) were estimated from the tests. The permeability is estimated according to flow measurements and Darcys' law. The porosity n of 0.48 is determined on the basis of the cylinder geometry and the built-in soil mass. For this porosity the critical hydraulic gradient of the soil sample i_{crit} is 0.86. Saturation is estimated from the measurements, according to a parameter optimization based on linear superposition of Terzaghis' analytical solution of the one-dimensional consolidation equation. For a more detailed look onto the soil parameters see Keese *et al.* (2026).

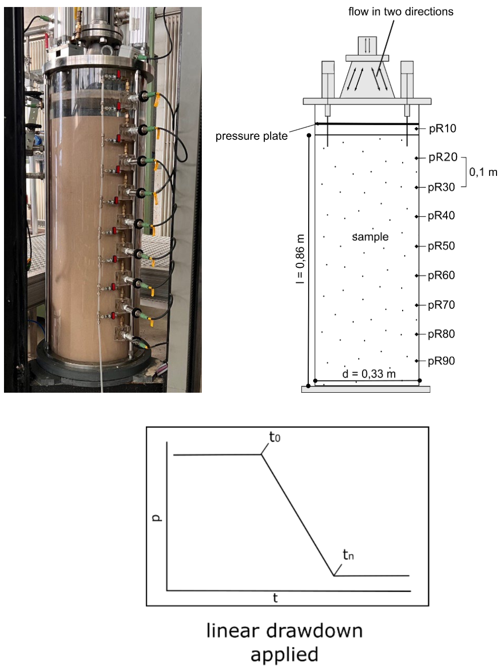

Figure 2 Test cell with soil sample (left), schematic drawing (right) and schematic linear pressure change (bottom).

Table 1 shows the individual tests and boundary conditions. The pressure levels for each test are given as mean pressure levels during the test. The study covers several external impact factors. These are:

The change in water depth (Tests No. V22/V26/V30), for these tests a typical water level drawdown of 0.6 m in 5 s triggered by ships is used at different pressure levels.

The change in drawdown velocity (Tests No. V22/V23/V24), where typical drawdowns of 0.6 m and 1.0 m are used but with an increasing drawdown velocity.

The change in total extend of the drawdown (Tests No. V33/V34/V35), where the drawdown velocity and end pressure level are constant in all tests (5 m), but the water level drawdown is extended in every test.

3.3 Exemplary analysis and limits of the test results based on Test No. V24

In the following section the analysis of the tests is shown as an example using test V24 and compared with the results of the same test with a load on top of the sample (V24_loaded), where no liquefaction occurs, to highlight the characteristics of a liquefied sample. The pressure sensors above (pR10) and along (pR20-pR90) the soil sample measure the absolute pressure. The excess pore water pressure Δp (kPa) for each sensor depth z_i (m) is then calculated from the pore water pressure $p_i(t)$ (kPa) less the pressure above the sample $p_{pR10}(t)$ (kPa) and the hydrostatic pressure component

$$\Delta p_i = p_i(t) - p_{pR10}(t) - \gamma_w \cdot z_i \quad (4)$$

A rapid water level drawdown leads to an increase in excess pore water pressure in the sample and a slow decrease at the end of the drawdown t_n (Figure 3, top). The maximum excess pore water pressures over the depth at the end of a drawdown are shown in Figure 3 (bottom) along with the vertical effective stresses $\sigma'_v = \gamma' z$ for the initial state at t_0 (before drawdown). For comparison, the limit effective stresses in the soil are shown, calculated with a minimum porosity σ'_{v,n_min} and maximum porosity σ'_{v,n_max}. The results show that the excess pore water pressures of V24 agree with the values of the vertical effective stresses in the upper part of the soil, which gives a first indication of liquefaction (see equation 1) in this part of the sample. In contrast, the excess pore water pressures in V24_loaded develop over a larger range, as the soil is subjected to a top load and a higher excess pore water pressure can built up as effective stresses are still greater than zero.

Table 1. Tests, boundary conditions and soil parameters

	Boundary conditions						Soil parameters	
Test No	**simulated water depth**	**mean pressure level**	**draw-down**	**pressure change**	**draw-down time**	**draw-down velocity**	**Permea-bility**	**Saturation**
			z_a		t_a	v_a	k	S_r
	[m]	[bar]	[m]	[bar]	[s]	[m/s]	[m/s]	[-]
V22	3	1.31	0.6	0.06	5.0	0.12	1.08E-04	0.91
V23	3	1.31	1.0	0.10	5.0	0.20	1.09E-04	0.92
V24	3	1.32	1.0	0.10	2.5	0.40	9.00E-05	0.94
V26	5	1.49	0.6	0.06	5.0	0.12	1.17E-04	0.92
V30	10	2.00	0.6	0.06	5.0	0.12	1.30E-04	0.95
V33	5	1.51	1.2	0.12	10.0	0.12	1.20E-04	0.93
V34	5	1.57	2.4	0.24	20.0	0.12	1.20E-04	0.93
V35	5	1.63	3.6	0.36	30.0	0.12	1.24E-04	0.93

As a next step, the hydraulic gradients i (-) are calculated by evaluating the pressure change between two sensors and their distance from one another

$$i = \frac{\Delta p_{i+1} - \Delta p_i}{z_{i+1} - z_i} \cdot \frac{1}{\gamma_w} \qquad (5)$$

If these are considered over the depth of a sample and compared to Terzaghis' critical hydraulic gradient i_{crit} (equation 3) further conclusions on a possible liquefaction can be made.

Figure 4 shows the hydraulic gradient over depth, as well as the boundaries for i_{crit}, calculated with n_{min} ($i_{crit,min} = 0.97$) and n_{max} ($i_{crit,max} = 0.82$) examined from bulk density lab tests for the given soil, where $n_{min} = 0.41$ and $n_{max} = 0.52$. It is helpful to compare the hydraulic gradient to these limits, since the porosity may change during a liquefaction. This process can be observed as the soil sample rises by a few millimetres during a drawdown, but the process cannot be quantified yet in terms of changing porosities. In test V24 the hydraulic gradient stays close to the critical limits in the upper part of the sample which indicates liquefaction, whereas in the lower part shows a rising gradient from bottom to mid-sample indicates a flow from the bottom. This is illustrated in Figure 4 (top and mid), where the gradients are presented over time (V24 only) and depth (V24 and V24_loaded).

As mentioned above, the formation of gradient plateaus can also be shown (i20 – i40). The test V24_loaded shows a rising hydraulic gradient from the bottom to the top indicating an ongoing upward flow. This is typical for a soil in which liquefaction is prevented, e.g. by an added load. Here hydraulic gradients greater than i_{crit} develop, as the flow forces generated lead to higher gradients (see Figure 4 mid).

Additionally, the vertical effective stresses (eq. 1) at the end of a drawdown t_n were calculated and plotted with the vertical effective stresses σ_v' at t_0 in Figure 4 (bottom). V24 shows effective stresses near zero in the upper part of the sample, according to the hydraulic gradients and excess pore water pressures, whereas slight negative stresses occur in the lower part. The negative stresses are calculated from the excess pore water pressures, which in Figure 3 (right) exceed the effective stresses in the lower area of the sample. Chowdhury *et al.* (2006) state that this is an indication of liquefaction.

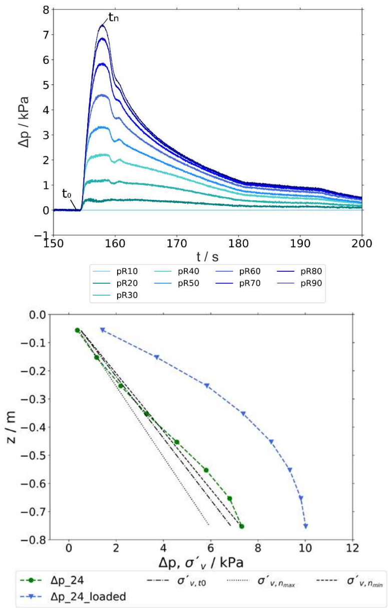

Figure 3: Excess pore water pressure over time (top) and maximum excess pore water pressure at the end of the drawdown over depth of the sample (bottom).

However, according to their work, the excess pore water pressures already increase in the upper part of the soil above the effective stresses. The observed effect could therefore also be due to the boundary conditions of the test cylinder. This would also be consistent with the hydraulic gradient values in the lower part of the sample. If liquefaction occurs here, these values would also be around i_{crit}. The reason why the zero value is not exactly achieved in the upper part is that a slight change in pore volume in the liquefied zone also leads to a change in unit weight.

However, as it is not yet possible to quantify exactly how large this change is and to what exact depth it extends. Thus, the initial unit weight of the soil is used to calculate the effective stresses, which leads to slight deviations of the values in the liquefied area around zero. The effective stresses of the non-liquefied sample cannot be shown in this figure because the specimen is held by a superimposed load, the exact value of which is not known. This results in an unknown initial stress in the specimen and the effective stresses cannot be recalculated.

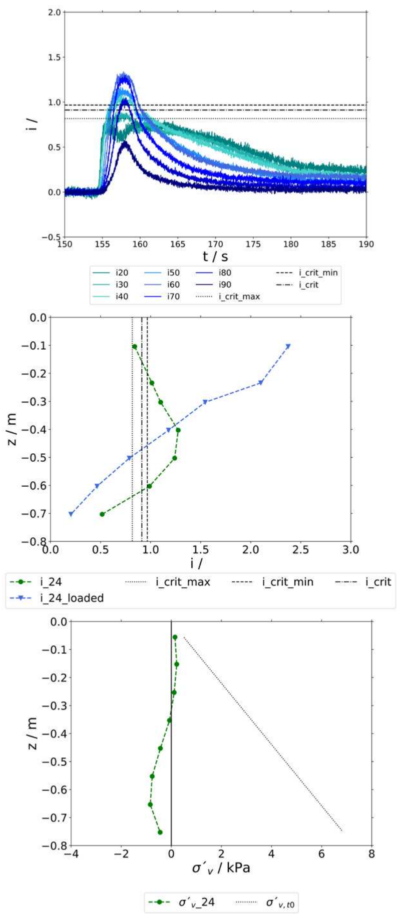

Figure 4: Hydraulic gradient over time for V24 (top), over depth (mid) and calculated vertical effective stresses over depth at the end of a drawdown (bottom).

4 RESULTS

The results of the test cases and the described boundary conditions in Table 1 are shown for each category. Therefore, the excess pore water pressure, the hydraulic gradient over depth and the vertical effective stresses over depth at the end of the drawdown are presented.

The tests with a change in water depth were performed with the same drawdown of 0.6 m in 5 s for each test, but at different pressure levels, representing different water depths of 3.0 m (V22), 5.0 m (V26) and 10.0 m (V30). By increasing the pressure level on the quasi-saturated soil, saturation starts to increase as well, as the gas gets compressed and the permeability increases slightly (Rothschink and Stelzer 2022). Due to a lower gas content and a higher permeability, lower excess pore water pressures and therefore less potential liquefaction occurs in the sample. This can be seen very well in the tests (see Figure 5), where V22 shows the highest excess pore water pressures and V30 the lowest. Besides, the excess pore water pressures of V30 do not correspond with the initial vertical effective stresses. Therefore, the potential of a liquefaction in V30 is not given, which is also evident in the evaluation of the hydraulic gradients and the calculated vertical effective stresses. V22 and V26 show hydraulic gradients around the critical hydraulic gradient limits and also effective stresses near zero in the upper part of the sample, which indicates a liquefaction to around -0.3 to -0.4 m for both tests.

In the tests with a change in drawdown velocity, typical drawdowns of 0.6 m and 1.0 m are used but with an increasing drawdown velocity from 0.12 m/s to 0.4 m/s. The results show, that the slow drawdown of V22 results in lower excess pore water pressure than V23 and V24 (Figure 6). Thus, the critical hydraulic gradient is only reached at the top of the sample and a liquefaction can be seen to around -0.3 to -0.4 m. V23 and V24 show about the same development of the excess pore water pressure as V22 in the upper part, but then develop higher excess pore water pressures. The hydraulic gradients exceed the critical hydraulic gradient, especially in the lower part but pressure measures and vertical effective stresses still show signs of liquefaction to around -0.3 to -0.4 m.

As described above for V24, the calculated vertical effective stresses for V23 and V24 have slight negative numbers due to the higher excess pore water pressures in the lower part of the sample. The fact that these two show very similar values may indicate a limit value that is related to the saturation or boundary conditions of the test cylinder.

The change in total extend of the water level drawdown is carried out with test V33, V34 and V35. These are varied in their total drawdown from 1.2 m (V33) over 2.4 m (V34) to 3.6 m (V35) with a constant drawdown velocity of 0.12 m/s. Here the pressure at the end of the drawdown was held to 1.5 bar in all tests and the starting pressure varied to create the pressure change. The aim is to determine whether a longer drawdown at the same drawdown velocity would lead to a further reaching liquefaction within the soil column. The results in Figure 7 show that the three different drawdowns lead to nearly the same results in the excess pore water pressure, hydraulic gradients and vertical effective stresses at the end of the drawdown. According to the used criteria, the hydraulic gradients of all three tests show signs of liquefaction in the upper and middle part of the soil sample and the vertical effective stresses show values at or around zero from the top of the sample to about -0.5 to -0.6 m. The hydraulic gradients in these tests clearly show that although the values do not exactly reach the critical hydraulic gradient, liquefaction is detected.

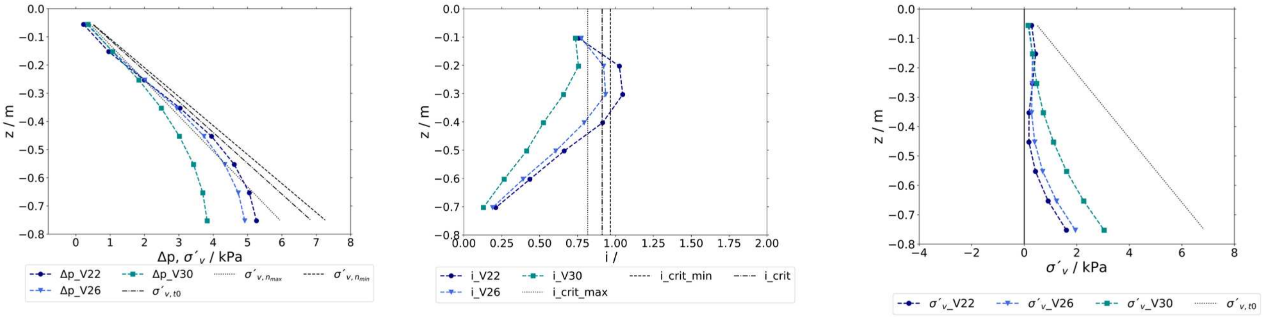

Figure 5: Excess pore water pressure (left), hydraulic gradient (mid) and vertical effective stresses (right) of the tests V22, V26, V30 varying the water depth.

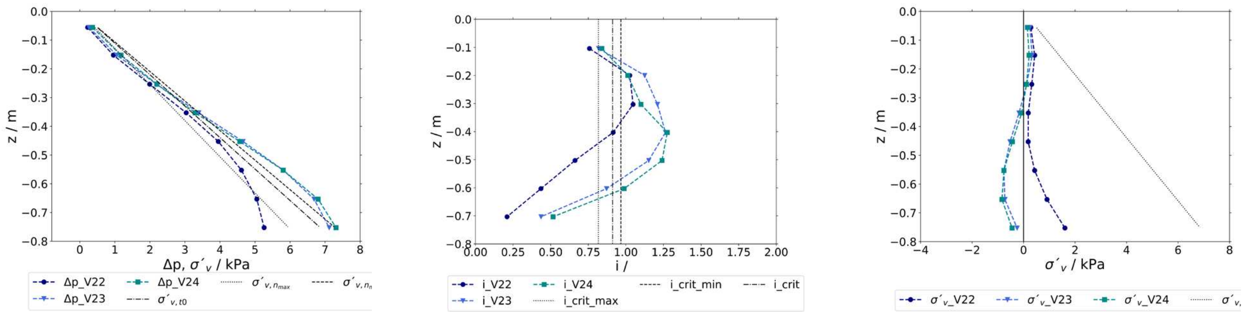

Figure 6: Excess pore water pressure (left), hydraulic gradient (mid) and vertical effective stresses (right) of the tests V22, V23, V24 varying the drawdown velocity.

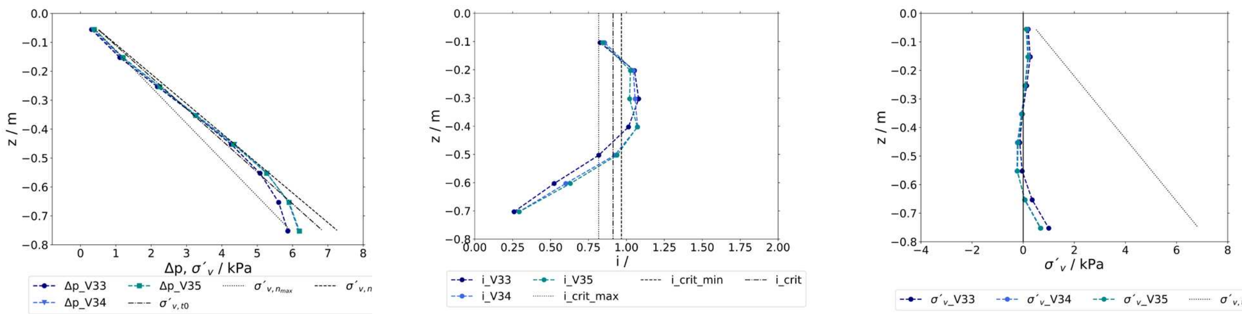

Figure 7: Excess pore water pressure (left), hydraulic gradient (mid) and vertical effective stresses (right) of the tests V33, V34, V35 varying the extend of the drawdown

5 DISCUSSION AND CONCLUSION

For the tests of the first group, the aim was, to show the impact of the water depth as a result of which the saturation changes. The tests with a shallow water depth have a lower saturation and a lower permeability than the tests with a deeper water depth. The water saturation in the tests ranges from 91 to 95 %. The excess pore water pressures reach higher values and the liquefaction depth is greater in the lower saturation test due to the higher gas content. Therefore, the potential for liquefaction is higher in soils with lower saturation, as shown in test V22. The tests V26 and V30 with gradually lower gas content and higher permeability show less to non-liquefaction according to the criteria used. The results show, that the water depth, which influences mainly the saturation, has an impact on the liquefaction potential of a soil.

The second group of tests were carried out at the same water depth but with a variation in the water level drawdown velocity. The results show, that especially in the upper part of the sample, the excess pore water pressures and therefore the liquefaction depth in the tests are almost similar to each other and liquefaction depth ranges from -0.3 to -0.4 m. In the lower part V23 and V24 reach higher excess pore water pressures, due to a higher drawdown velocity, which leads to slight negative effective stresses calculated in the lower part of the sample. This effect may occur due to the boundary conditions of the test cylinder but at the moment this effect has not yet been fully resolved. For this purpose, it would be important to carry out liquefaction tests in larger test facilities like the river bed simulator at the Federal Waterways Research and Engineering Institute.

For the third group, a change in the water level drawdown was chosen to be varied. The drawdowns range from 1.2 m over 2.4 m to 3.6 m with a constant drawdown velocity of 0.12 m/s and a varying drawdown time ending at a water depth of 5 m. The permeability and saturation have approximately the same value in all three tests. The results show nearly the same depth of liquefaction in all three tests whereby it can be assumed that the depth and duration of a water level drawdown in this case, is not necessarily decisive for the extend of the liquefaction.

The results of this study show, that linear water level drawdowns in fine sands can lead to momentary soil liquefaction according to the criteria used. Depending on the boundary conditions and external impact factors, liquefaction can take place in the upper part of the sample or extend to greater depths. The measured excess pore water pressures and the resulting calculated critical hydraulic gradients and vertical effective stresses are used to evaluate the depth in which liquefaction occurs. However, the values in the calculation are very sensitive and small variations in the pressure measurements can lead to fluctuations in the gradients, so that the critical gradients are exceeded or undershot despite liquefaction. There are also some limitations that cannot be fully resolved in the tests at this time. These include the boundary influences of the test cylinder or the change in porosity during the liquefaction. The latter causes a change in the unit weight of the soil. Although an uplift of the soil can be observed in the tests, it is not yet possible to quantify in which part of the soil column this occurs or whether the whole sample expands homogeneously. Future tests will focus on these aspects. A numerical approach to the influences of the test cell geometry and soil parameters are investigated in Keese *et al.* (2026).

REFERENCES

Chowdhury, B., Dasari, G.R., and Nogami, T., 2006. Laboratory Study of Liquefaction due to Wave–Seabed Interaction. *Journal of Geotechnical and Geoenvironmental Engineering*, 132 (7), 842–851. https://doi.org/10.1061/(ASCE)1090-0241(2006)132:7(842)

Ewers, J., 2019. Laboratory tests on the effects of wave action on cohesionless soil and their influence on incipient sediment motion. *Scour and Erosion IX – Keh-Chia (Ed.)*, 511–518. https://doi.org/10.1201/9780429020940-72

Federal Waterways Engineering and Research Institute, ed., 2010. *BAW Code of Practice: Principles for the Design of Bank and Bottom Protection for Inland Waterways (GBB)*. Karlsruhe: Federal Waterways Engineering and Research Institute.

Fredlund, D.G., 1976. Density and compressibility characteristics of air–water mixtures. *Canadian Geotechnical Journal*, 13 (4), 386–396. https://doi.org/10.1139/t76-040

Kayser, J., *et al.*, 2016. A Test Apparatus for Alternating Flow in Geotechnical Engineering. *Geotech. Test. J. (Geotechnical Testing Journal)*, 39 (5), 865–878. https://doi.org/10.1520/GTJ20150252

Keese, H., *et al.*, 2026. Parameter study of factors influencing wave-induced liquefaction. *Proceedings of the 11th International Conference on Physical Modelling in Geotechnics*.

Köhler, H.-J., 1997. Boden und Wasser - Druck und Strömung. *Soil and water - pressure and flow. BAW Mitteilungen*, 76, 15–33.

Nago, H., 1981. Liquefaction of highly saturated sand layer under oscillary water pressure. *Memoirs of the School of Engineering Okayama University* (16), 91–104.

Rothschink, J. and Stelzer, O., 2022. Ship wave induced excess pore water pressure in riverbeds and banks – an investigation on silty sands. *11th River Flow Conference*, 301–308.

Sakai, *et al.*, 1992. Wave-Induced Effective Stress in Seabed and Its Momentary Liquefaction. *Journal of Waterway, Port, Coastal and Ocean Engineering*, 118 (2), 102–106. https://doi.org/10.1061/(ASCE)0733-950X(1992)118:2(202)

Skempton, A.W., 1954. The Pore-Pressure Coefficients A and B. *Géotechnique* (4), 143–147. https://doi.org/10.1680/geot.1954.4.4.143

Terzaghi, K., Peck, R.B., and Mesri, G., 1967. *Soil Mechanics in Engineering Practice.* 3rd ed. New York: Wiley & Sons.

Zen, K. and Yamazaki, H., 1990. Mechanism of Wave-Induced Liquefaction and Densification in Seabed. *Soils and Foundations*, 30 (4), 90–104. https://doi.org/10.3208/sandf1972.30.4_90